



Transfer learning for enhancing the homogenization-theory-based prediction of elasto-plastic response of particle/short fiber-reinforced composites

Jiyoung Jung^a, Yongtae Kim^a, Jinkyoo Park^b, Seunghwa Ryu^{a,*}

^a Department of Mechanical Engineering, Korea Advanced Institute of Science and Technology (KAIST), 291 Daehak-ro, Yuseong-gu, Daejeon 34141, Republic of Korea

^b Department of Industrial & Systems Engineering, Korea Advanced Institute of Science and Technology (KAIST), Daejeon 34141, Republic of Korea



ARTICLE INFO

Keywords:

Homogenization
Transfer learning
Adaptive incrementally affine
Short fiber-reinforced composite
Machine learning
Deep Neural Network

ABSTRACT

Mean-field homogenization methods relying on the solution of Eshelby's inclusion problem do not provide accurate predictions when the interaction among reinforcements becomes significant, or in the inelastic response regime when the shape of the reinforcement has a high aspect ratio. Herein, we propose a combined theoretical and data-driven approach in which a homogenization method is followed by transfer learning to enhance the prediction of the nonlinear mechanical response of particle/short fiber-reinforced composites. We trained a deep neural network (DNN) with a massive stress-strain curve dataset of the composites subjected to uniaxial and cyclic loading in the elasto-plastic regime based on the adaptive incrementally affine homogenization method; then, we fine-tuned the pre-trained DNN via transfer learning with a relatively small dataset based on time-consuming three-dimensional (3D) finite element analyses (FEA). The transfer learning approach exhibited better predictive performance than the DNN directly trained only with the FEA dataset did, for a wide range of reinforcement volume fractions and shapes. With transfer learning, the DNN exploits the knowledge learned from the homogenization theory to perform new learning tasks on small datasets from 3D FEA. The proposed approach can be extended to other composite analyses requiring excessive time and cost for large datasets.

1. Introduction

With the addition of various forms of reinforcements, reinforced composites have evolved to outperform single-phase materials. Predictions of the effective responses of such composites are crucial for efficient machine element design and structural optimization across a variety of industries. As the first generation of composite analysis, homogenization methods based on analytical formulations have been investigated in the past [1,2]. These methods entail lower computational costs compared with finite element analysis (FEA) or experiments but have limitations owing to the use of mathematical assumptions. For example, the mean-field homogenization theory is valid under a relatively small volume fraction of reinforcement (<20%) because the mean-field assumption is violated as the volume fraction increases [3–6]. If a homogenization method relies on the solution of Eshelby's inclusion problem, reinforcements with a non-ellipsoidal shape can only be approximately treated [7–9]. As the second generation of composite analysis, the finite element method (FEM) has been extensively

employed with the advancement of computational capability [10]. However, the nonlinear behavior of materials and structural complexity significantly increase the computational cost of the FEM, which limits its applicability. Recently, as the third generation of composite analysis, data-based machine learning [11,12], which incorporates machine learning techniques into the composite analysis [13–16], has drawn significant attention. Once a machine learning model has been trained, it can immediately predict the outputs for given input values; however, it requires a large amount of data for reliable prediction.

Each method has advantages and disadvantages, and thus, a single method would not be a satisfactory or universal route toward efficient composite analyses. For example, the homogenization theory enables exceedingly fast prediction of the effective properties of composites, but its accuracy and applicability are limited. Meanwhile, both three-dimensional FEM analysis and direct experimental measurements offer highly accurate predictions of composite properties but at the expense of computational cost and time. However, the accuracy and efficiency of composite analysis can be significantly improved by training a machine

* Corresponding author.

E-mail address: ryush@kaist.ac.kr (S. Ryu).

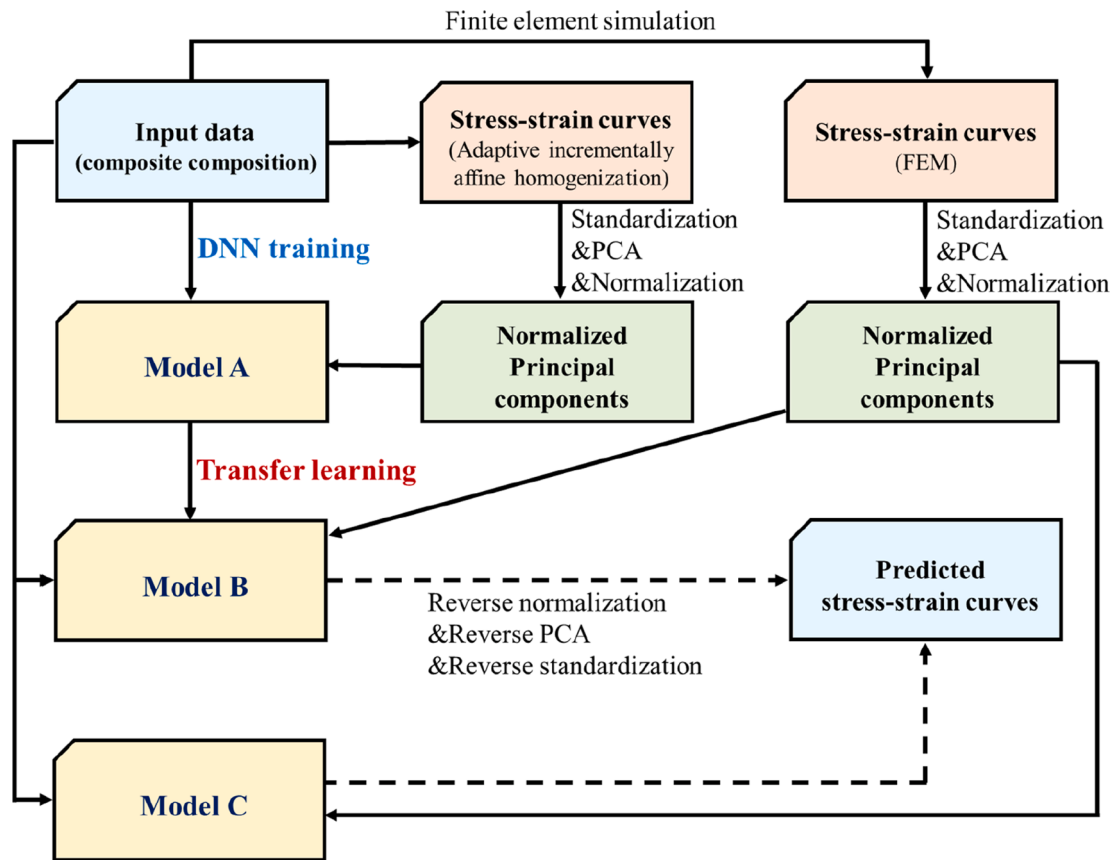


Fig. 1. The overall workflow for transfer learning. Model A was trained using a significantly large homogenization dataset at a low computational cost. Applying transfer learning, Model B was fine-tuned with a relatively small FEM dataset using Model A as a starting point. Model C refers to the model trained only based on the FEM dataset. To verify the superiority of transfer learning approach, the performances of Models B and C were compared.

learning model with a large but less accurate dataset based on the homogenization method and then improving the machine learning model with an accurate but small dataset using the FEM or through experiments. Herein, we propose a combined theoretical and data-driven framework to realize such a hybrid composite analysis via transfer learning.

Various mean-field homogenization methods have been proposed based on Eshelby's solution [1]. For linear elastic composites, the Mori-Tanaka [2,17], differential [18,19], and double-inclusion [20] methods have been widely used. For composites exhibiting nonlinearity, such as viscosity or plasticity, the incrementally affine [21,22], incrementally secant [23,24], and adaptive incrementally affine [25,26] methods have been proposed. These methods are reliable when the shape of the reinforcement is close to a sphere and the volume fraction of the reinforcement is small. However, many technologically important composites are synthesized with a variety of forms and a relatively large volume fraction of reinforcement, which limits the applicability of homogenization methods. In contrast, deep learning techniques have been employed to predict the mechanical properties of two-dimensional checkerboard composites [15,27–29] or three-dimensional linear elastic composites [30,31]. It is well known that with more data, the generalization of a deep neural network (DNN) model is improved for unseen data. When a sufficiently large training dataset does not exist, the performance of DNNs becomes inferior to that of conventional machine learning techniques such as linear regression, support vector machine, or decision tree-based algorithms [16]. However, it is often difficult to obtain sufficiently large datasets owing to time and cost problems.

Given that homogenization methods have limitations in terms of accuracy and that DNNs require excessively large amounts of data, we

propose incorporating transfer learning techniques to composite analysis. Transfer learning is a method that uses a model trained once for a particular task as a starting point for training a second model [32]. Therefore, transfer learning is used when it is difficult to obtain sufficient data [33–37]. The representative volume element (RVE) of a composite with reinforcements having a high aspect ratio in the nonlinear regime entails substantial computational costs associated with FEM; then, it becomes difficult to obtain the amount of data required for machine learning. In the present study, we show that a framework combining the homogenization theory and transfer learning can predict the effective behavior of the elasto-plastic composite efficiently and reliably; a sufficiently large dataset is generated using the homogenization theory for the initial DNN training, at a low computational cost; subsequently, the pre-trained DNN is fine-tuned using relatively small FEM data obtained via transfer learning. The workflow of our transfer-learning framework is illustrated in Fig. 1.

The remainder of this paper is organized as follows. The constitutive equations for modeling the elasto-plastic behavior are summarized in Section 2.1. A description of the data generation is presented in Section 2.2. The adaptive incrementally affine and yield reduction methods are briefly introduced for the homogenization data. The face-centered-cubic (FCC) structured RVE is introduced for FEM data. The procedure for applying transfer learning is described in Section 3. The results for the ellipsoidal particle-reinforced composite are presented in Section 4.1. The results for the short fiber-reinforced composites are included in Section 4.2. The results for the ellipsoidal particle-reinforced composite under cyclic loading are shown in Section 4.3. The conclusions are presented in Section 5.

Boldface letters indicate second- or fourth-order tensors and non-bold face letters indicate scalar values; (:) denotes a double contraction.

Table 1

Input parameters with given ranges for elasto-plastic composites.

ν_0	σ_y/E_0	k/E_0	n	E_1/E_0	ν_1	AR	f_1
0.1 ~	0.005 ~	0.01 ~	0.2 ~	1 ~	0.1 ~	1 ~	1%
0.45	0.025	0.1	0.6	200	0.45	10	~30%

$$\mathbf{a} : \mathbf{b} = a_{ij}b_{ji}; \quad (\mathbf{A} : \mathbf{b})_{ij} = A_{ijkl}b_{lk}$$

2. Material modeling and numerical method

2.1. Material modeling

We consider composites containing an elasto-plastic matrix. We note that the methodology employed in this study can be applied to a variety of other composite materials as well that show viscoelastic or viscoelastic-viscoplastic responses. In the elasto-plastic constitutive model, the total strain ($\boldsymbol{\epsilon}$) is divided into the elastic part ($\boldsymbol{\epsilon}^e$) and plastic part ($\boldsymbol{\epsilon}^p$):

$$\boldsymbol{\epsilon} = \boldsymbol{\epsilon}^e + \boldsymbol{\epsilon}^p. \quad (1)$$

Then, the Cauchy stress ($\boldsymbol{\sigma}(t)$) is determined as follows:

$$\boldsymbol{\sigma}(t) = \mathbf{C} : \boldsymbol{\epsilon}^e = \mathbf{C} : (\boldsymbol{\epsilon} - \boldsymbol{\epsilon}^p). \quad (2)$$

Assuming isotropic materials, the fourth-order stiffness tensor (\mathbf{C}) is expressed as,

$$C_{ijkl} = \frac{E\nu}{(1-2\nu)(1+\nu)}\delta_{ij}\delta_{kl} + \frac{E}{2(1+\nu)}(\delta_{ik}\delta_{jl} + \delta_{il}\delta_{jk}), \quad (3)$$

where E is Young's modulus, ν is Poisson's ratio, and δ is the Kronecker delta.

Rate-independent isotropic hardening is assumed for plasticity. The yield function (f) is defined as follows:

$$f(\sigma_{eq}, p) \equiv \sigma_{eq} - (\sigma_y + R(p)) \text{ where } \sigma_{eq} = \sqrt{\frac{3}{2}s : s} \quad (4)$$

$$p(t) \equiv \int_0^t \dot{p}(\tau) d\tau \text{ where } \dot{p}(\tau) = \sqrt{\frac{2}{3}\dot{\boldsymbol{\epsilon}}^p(\tau) : \dot{\boldsymbol{\epsilon}}^p(\tau)}, \quad (5)$$

where s is the deviatoric part of the Cauchy stress, σ_{eq} is the von Mises stress, σ_y is the yield stress, R is the hardening stress, and p is the accumulated plastic strain. For hardening responses beyond the yield, isotropic hardening with the power law is adopted:

$$R(p) = kp^n \quad (6)$$

where k is the hardening modulus, and n is the hardening exponent. Thus, isotropic elasto-plastic behavior can be modeled with five parameters: Young's modulus, Poisson's ratio, yield stress, hardening modulus, and hardening exponent.

2.2. Data generation with a homogenization method and 3D FEM modeling

Considering that the reinforcements are much stiffer than the matrix materials in most composites, the composite is assumed to be an elasto-plastic matrix reinforced with linear elastic particle/short fiber. Its composition can be characterized by nine parameters related to the elastic properties (Young's modulus E_0 , Poisson's ratio ν_0) and plastic properties (yield stress σ_y , hardening modulus k , hardening exponent n) of the matrix, as well as the elastic properties (Young's modulus E_1 , Poisson's ratio ν_1), aspect ratio (AR), and volume fraction (f_1) of the reinforcements. After normalizing E_1, σ_y , and k with E_0 , the input parameters can be reduced to a set of eight dimensionless parameters. With the normalized eight parameters as the input, we set the effective stress-

strain curve of the composite subjected to uniaxial loading as the output. We consider a wide range of input parameters to cover a variety of elasto-plastic composite behaviors, as presented in Table 1.

The adaptive incrementally affine method with yield reduction is adopted as the homogenization method because it has been shown to offer highly accurate predictions of the complex nonlinear mechanical response of particulate-reinforced composites beyond the elastic regime, under cyclic and multiaxial loading. In the regime where the assumption of micromechanics-based mean-field homogenization theory holds, that is, a small volume fraction of a reinforcement having an ellipsoidal shape with an aspect ratio close to 1, the adaptive incrementally affine method offers highly accurate predictions; however, its accuracy is diminished with an increase in the reinforcement volume fraction or aspect ratio.

The complete details of the homogenization method can be found in our previous studies [25,26]; we provide some of these details herein for clarity. The yield reduction method reduces the yield stress of the matrix with the volume fraction of the reinforcement.

$$\sigma_y \leftarrow (1-f_1)\sigma_y \text{ for the matrix} \quad (7)$$

The adaptive incrementally affine method for elasto-plastic composites is summarized as follows. Here, subscripts 0 and 1 represent variables of the matrix and reinforcement, respectively (e.g., C_0 refers to the stiffness tensor of the matrix and C_1 refers to the stiffness tensor of the reinforcement).

1. A macro-strain increment ($\Delta\bar{\boldsymbol{\epsilon}}$) is applied to the composite for a given strain state at t_n .
2. The strain increment of the reinforcement is initialized as a macro-strain increment:

$$\langle \Delta\boldsymbol{\epsilon} \rangle_{w_1} = \Delta\bar{\boldsymbol{\epsilon}}$$

where $\langle \cdot \rangle_{w_0}$ and $\langle \cdot \rangle_{w_1}$ refer to the volume averages over the matrix and particles, respectively.

3. The strain increment of the matrix is calculated as follows:

$$\langle \Delta\boldsymbol{\epsilon} \rangle_{w_0} = \frac{1}{f_0}(\Delta\bar{\boldsymbol{\epsilon}} - f_1\langle \Delta\boldsymbol{\epsilon} \rangle_{w_1}). \quad (8)$$

where f_0 is the volume fraction of the matrix ($f_0 + f_1 = 1$).

4. Eshelby's tensor (S) [1,38] and the concentration tensors (B_1^e, A_1^e) are computed as follows:

$$B_1^e = [\mathbf{I} + S : (C_0)^{-1} : (C_1 - C_0)]^{-1} \quad (9)$$

$$A_1^e = B_1^e : (f_0\mathbf{I} + f_1B_1^e)^{-1} \quad (10)$$

where \mathbf{I} is the fourth-order identity tensor.

5. The residual tensor (R) is computed as follows:

$$\begin{aligned} R = & A_1^e : \Delta\bar{\boldsymbol{\epsilon}} - \langle \Delta\boldsymbol{\epsilon} \rangle_{w_1} + (A_1^e - \mathbf{I}) : (C_1 - C_0)^{-1} : (\sigma_1(t_{n+1}) - C_1 \\ & : \boldsymbol{\epsilon}_1(t_{n+1}) - \sigma_0(t_{n+1}) + C_0 : \boldsymbol{\epsilon}_0(t_{n+1})) + (\mathbf{I} - A_1^e) : (\mathbf{I} - B_1^e)^{-1} \\ & : [B_1^e : C_0^{-1} : \sigma_0(t_n) - C_1^{-1} : \sigma_1(t_n)] \end{aligned} \quad (11)$$

- 6-1. If $|R| > tolerance$, step 3 is repeated with a new trial.

$$\langle \Delta\boldsymbol{\epsilon} \rangle_{w_1} \leftarrow \langle \Delta\boldsymbol{\epsilon} \rangle_{w_1} + R \quad (12)$$

- 6-2. If $|R| < tolerance$, then step 7 is followed.

7. The macro stress increment ($\Delta\bar{\boldsymbol{\sigma}}$) and effective stiffness tensor ($\bar{\mathbf{C}}$) are obtained as follows:

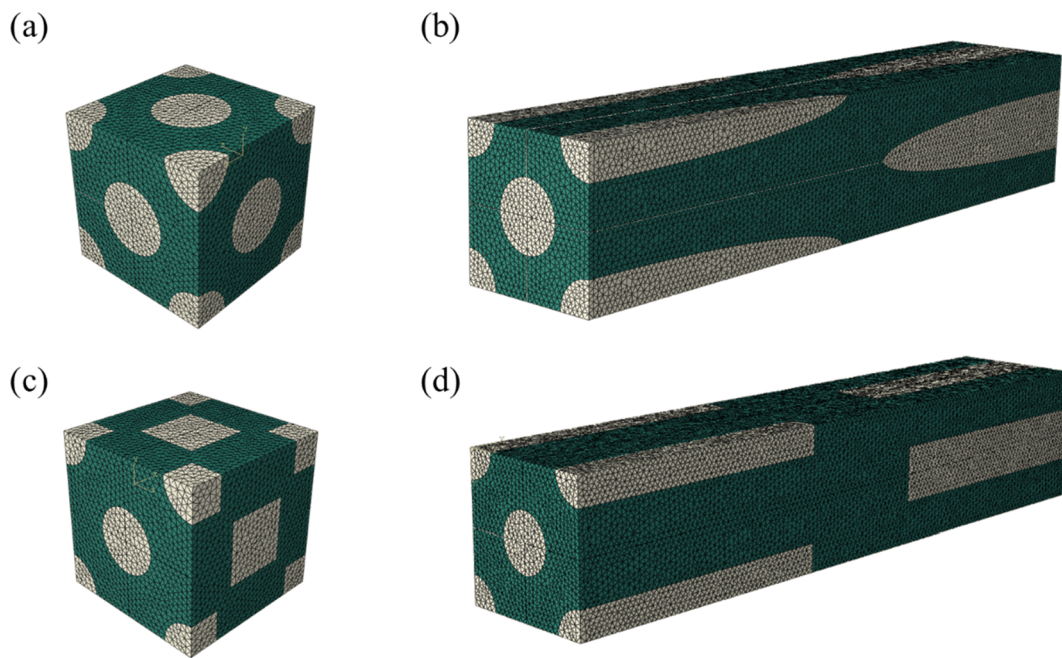


Fig. 2. FCC-structured RVE for FEM. (a, b) Spherical particle and ellipsoidal particle-reinforced composite, respectively. (c, d) Composite containing short fiber-reinforcements with aspect ratios of 1 and 10, respectively. (b, d) Half of FCC unit cell structure. Volume fractions of reinforcements are 20%.

$$\Delta\bar{\sigma} = f_0 \mathbf{C}_0 : (\langle \Delta\epsilon \rangle_{w_0} - \Delta\epsilon_0^p) + f_1 \mathbf{C}_1 : (\langle \Delta\epsilon \rangle_{w_1} - \Delta\epsilon_1^p). \quad (13)$$

$$\bar{\mathbf{C}} = [f_0 \mathbf{C}_0 + f_1 \mathbf{C}_1 : \mathbf{B}_1^e] : [f_0 \mathbf{I} + f_1 \mathbf{B}_1^e]^{-1}. \quad (14)$$

8. Step 1 is repeated for the next macro-strain increment.

The predictions of the adaptive incrementally affine method for elasto-plastic composites (metal matrix composites [39]) reinforced with spherical particles are compared with those of the original incrementally affine method in Supplementary Note 1 (see [Supplementary Information](#)). The original incrementally affine method which was implemented in the DIGIMAT software [40] is applied based on the formulation introduced in a previous study [21]. Under a given reinforcement volume fraction, the prediction accuracy of the homogenization method decreases as the aspect ratio of an ellipsoidal particle increases; this is because the mutual interaction among reinforcements increases, which further violates the mean-field assumption [22,39]. Additionally, the prediction provided by the homogenization method has another source of error for cylindrical short fiber-reinforced composites because Eshelby's solution assumes an ellipsoidal shape for the reinforcement.

The FEM offers an accurate numerical evaluation of the internal stress distribution and yield inside a composite under mechanical loading, and the outcome from the FEM can be considered as a ground truth if the implementation and numerical method are carefully executed. We employed the commercial software ABAQUS [41] with the UMAT code for the FEM simulations in this study. FEM data were generated considering the RVE; the reinforcement was embedded into an FCC configuration, as shown in [Fig. 2](#). Periodic boundary conditions should be considered for RVE to represent the behavior of bulk composites [42–44]. The analysis was conducted using only one-eighth of the RVE and symmetric boundary conditions were applied to all sides of the segmented RVE. Depending on the aspect ratio and volume fraction of the reinforcement, approximately 15,000 to 108,000 elements are required to ensure convergence. One can use RVEs with randomly distributed reinforcements instead of FCC-structured RVE. The stress-strain curves from those RVEs were compared with that of FCC-structured RVE under uniaxial tension in [Supplementary Note 2](#) (see

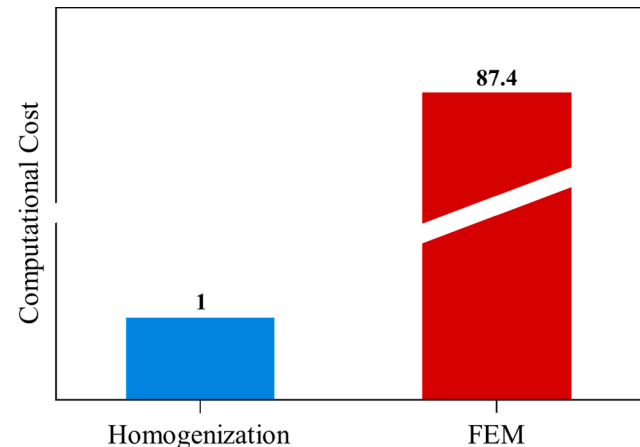


Fig. 3. Comparison of computational cost between homogenization method and FEM. The computational cost was defined by multiplying the computational time by the number of cores used in the simulation.

[Supplementary Information](#)). Noteworthy is that a sufficient number of reinforcements must be used to reduce the stress-strain curve variation which originates from the randomness of reinforcement distributions. One can model reinforcements with complex shapes instead of ellipsoidal/fiber-reinforcements but with finer mesh. Hence, considering RVEs involving randomly distributed or complex-shaped reinforcements requires a higher computational cost, emphasizing the need for an efficient transfer learning approach combined with the homogenization theory. Because this study aims to primarily show the validity of the transfer learning approach, the randomness of reinforcement distributions or the shape of reinforcements will be considered in our future study.

The computational costs for the homogenization method and FEM for the analysis of the composite are compared in [Fig. 3](#). Here, we consider composites containing reinforcements with an aspect ratio of 10, while the other input parameters are randomly assigned. For analyzing 100 composites, the homogenization method requires 5.2 h of

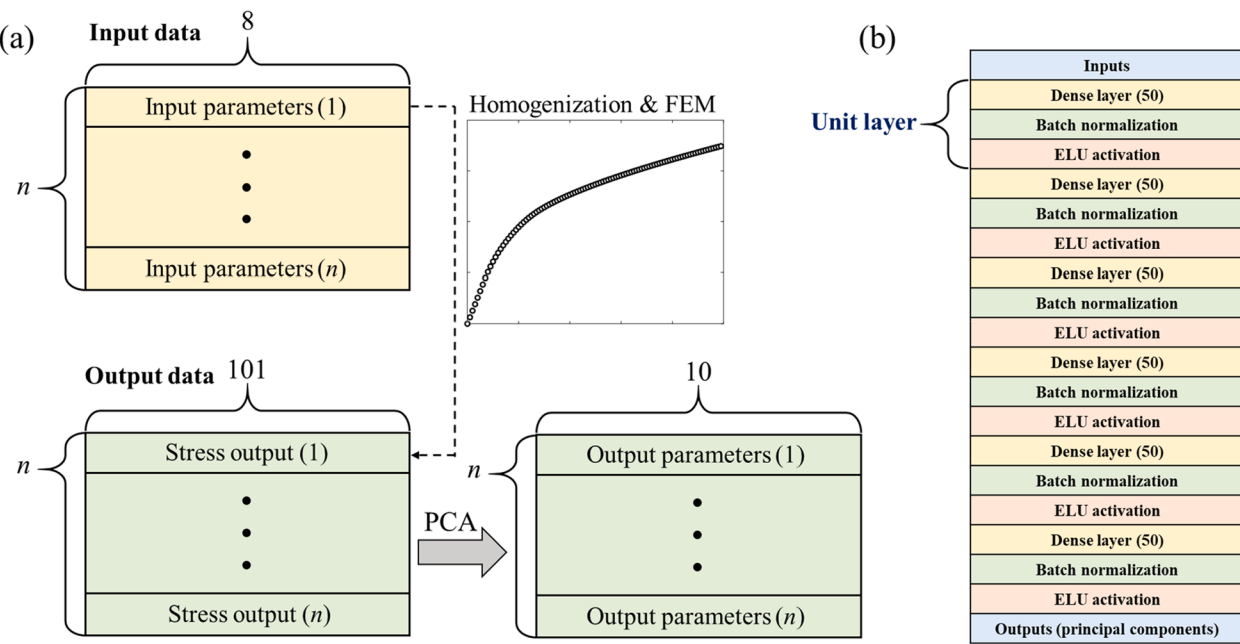


Fig. 4. (a) Data format of input (composite composition) and output stress-strain curve data. 101-dimensional stress data was compressed into 10-dimensional data via PCA. (b) DNN architecture was composed of six unit layers.

single-core computation, whereas the FEM needs 56.8 h of eight-core computation; thus, the FEM is 87.4 times more expensive than homogenization in terms of computational cost. Considering a variety of input parameter sets, the predictions provided by the adaptive incrementally affine method are compared with the FEM results for the ellipsoidal-particle/short fiber-reinforced composites in Fig. S3 (see Supplementary Information). Predictions from the homogenization methods show notable errors when the aspect ratio of the reinforcement or volume fraction is large. Moreover, although the FEM results are considered as ground truth in this study, experimental data (which also account for the effects from various manufacturing defects) can be used in the transfer learning scheme as well; this is discussed in the following section.

3. Application of transfer learning

Transfer learning has been widely used to train a task-specific model effectively by utilizing a pre-trained model with a massive dataset. Transfer learning can achieve powerful predictive performance even with a small amount of task-specific data by fine-tuning a subset of layers of the pre-trained model while typically freezing the feature extraction layers. In this study, we first pre-trained a DNN model with sufficient homogenization data to enable this pre-trained model to capture the underlying mechanism determining the effective stress-strain relationship for idealized ellipsoidal particle-reinforced composites. We then used task-specific data (FEM data) to fine-tune the pre-trained model for predicting the stress-strain relationship for an ellipsoidal-particle/short fiber-reinforced composite. For the fine-tuning procedure, unlike in typical transfer learning, we trained the task-specific model with FEM data using the parameters of the pre-trained model as the initial parameters, instead of freezing subset layers from the pre-trained model. We found that freezing some subsets degrades the performance of the fine-tuned DNN. This is because the knowledge that we seek to transfer is not an abstract feature but rather the general input and output structural relationships that are believed to be embedded in the overall layer of the pre-trained model. As shown in Fig. S4 (see Supplementary Information), the pre-trained model represents the general structure of the stress-strain curves well (the outputs are concave and monotonic functions).

The overall workflow of the transfer-learning framework is illus-

trated in Fig. 1. As depicted in Fig. 1, Model A was trained using the large dataset from the homogenization method with a low computational cost. Taking Model A as the initial point, Model B was fine-tuned using a small FEM dataset, which entailed a relatively high computational cost. On the other hand, Model C was trained only with the small FEM dataset. The DNN was constructed and trained using Keras [45] on Python 3.7. We first generated 59,500 stress-strain curve data using the homogenization method. We then constructed 2000 stress-strain curve data from computationally expensive FEM simulations. The homogenization data were divided into training and validation sets in a ratio of 49,000:10,500. The FEM data were divided into training, validation, and test sets in a ratio of 1400:300:300. The validation set was used as an early stopping criterion for training the DNN, and the test set was used for assessing the model. Each input parameter listed in Table 1 is normalized to values between 0 and 1. The output data, i.e., the stress-strain curves evaluated at 101 strain points (i.e., the dimension of the output is 101), are compressed into 10-dimensional vectors comprising the 10 most important principal components extracted via principal component analysis (PCA), as depicted in Fig. 4 (a), according to a previously proposed scheme [15]. The cumulative explained variance, which is defined as the sum of eigenvalues normalized by the sum of all eigenvalues ($\sum_{i=1}^{10} \lambda_{ii} / \sum_{i=1}^{101} \lambda_{ii}$) is 99.999%. The data that are dimensionally reduced via PCA, i.e., the 10 most important principal components, are normalized to values between 0 and 1 for efficient training. We chose a DNN architecture, which does not impose any structural assumption (inductive biases), to employ as flexible a model as possible to express the complex stress-strain relationship of elasto-plastic composites. A dense layer, batch normalization, and activation function constitute a unit layer in the DNN architecture as shown in Fig. 4 (b). Batch normalization is known to accelerate training, mitigate the sensitivity to initial weights, and have a regularization effect [46,47]. The weighted mean squared error (WMSE) is defined for DNN training as follows:

$$\text{WMSE} = \frac{1}{n} \sum_{i=1}^n \sum_{j=1}^{10} \sqrt{\lambda_{jj}} (Y_{j,i}^{\text{true}} - Y_{j,i}^{\text{pred}})^2 \quad (15)$$

where $Y_{j,i}$ refers to the j-th principal component of the i-th sample, λ_{jj} refers to the j-th eigenvalue, and n refers to the number of samples. The

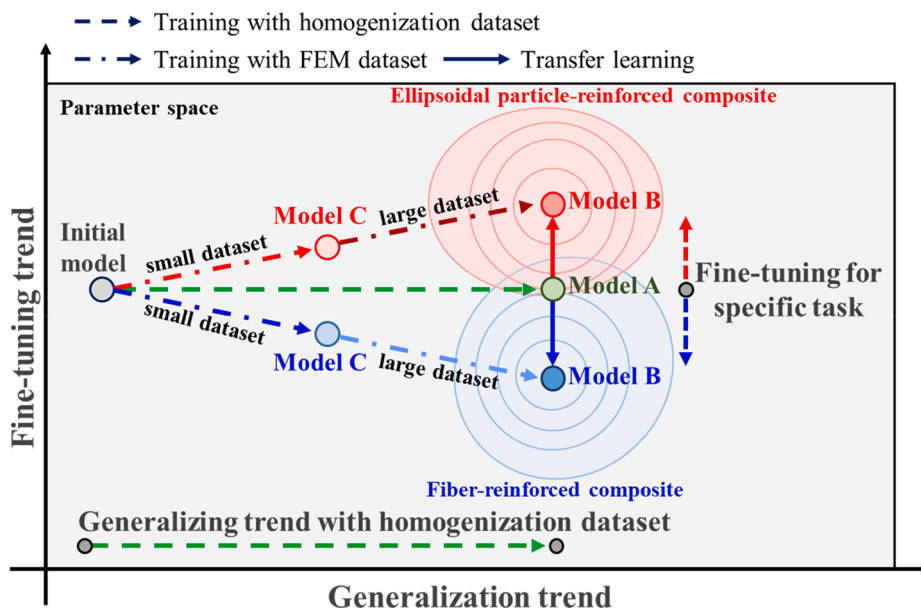


Fig. 5. Schematic of how transfer learning shows better performance. The initial model was set with random weights. Pre-training with a large homogenization dataset allowed DNN to capture the underlying mechanism between input and output. The transfer learning enabled the model to be fine-tuned from Model A based on homogenization theory. Model C suffered from overfitting owing to a lack of data.

variation between eigenvalues is exceedingly high; hence, the square root of the eigenvalues are used as weights. To optimize the DNN architecture, grid-search hyper-parameter tuning is performed to search for the best combination of the number of unit layers, the number of neurons in each layer, and the type of activation function [48–50]. We chose the architecture with the lowest average error after five epochs in the following search space (see Supplementary Note 3).

Number of neurons of each layer = [40, 50, 60, 70, 80, 90, 100, 110, 120]

Number of hidden unit layers = [3, 4, 5, 6, 7]

Activation function = [ReLU, GeLU, ELU, LeakyReLU]

The best architecture has 50 neurons for each layer, six hidden unit layers, and exponential linear unit (ELU) as an activation function as shown in Fig. 4 (b); this leads to 14,010 trainable parameters. The Adam optimizer, an adaptive learning rate optimizer, was used for training [51]. The batch size was set to one-tenth of the training dataset size. After each epoch, the training dataset was randomly shuffled to minimize the sample bias. After the training, based on the trained model, 101-dimensional stress-strain curves were recovered from 10-dimensional principal component arrays via reverse normalization and reverse PCA. Hereinafter, Model A refers to a DNN model trained with homogenization data, Model B represents a DNN model trained via transfer learning based on both homogenization data and FEM data, and Model C indicates a DNN model trained only with FEM data.

Neural networks must have sufficient width, depth, and trainable parameters when the relationship between the input and output is complex. In such circumstances, a large amount of data is required for the DNN to achieve satisfactory generalization performance (i.e., prediction of unseen data). Training with a small amount of data would lead to an over-fitted model with poor generalization. The transfer learning strategy proposed in this study is illustrated in Fig. 5. The x-axis represents how general knowledge is extracted from the abundant homogenization data through pre-training. Owing to the abundance of the homogenization data, the pre-trained model becomes sufficiently general to serve as a structural foundation for various task-specific models. The y-axis represents how the pre-trained model is fine-tuned using FEM data to form task-specific models. Model C suffers from overfitting

owing to the lack of data, especially when using a flexible DNN architecture. Meanwhile, Model A cannot accurately predict the task-specific stress-strain relationship of composites, because of the limitation of the homogenization theory. Despite the difference between the predictions provided by homogenization and the FEM, these predictions share the underlying mechanism determining the effective stress-strain relationship. We believe that Model A captures the underlying mechanism based on the homogenization theory. Relying on the general stress-strain relationships extracted from the pre-trained model, Model B can be quickly adapted for ellipsoidal-particle/short fiber-reinforced composites, avoiding overfitting, even when using a small amount of task-specific FEM data. In summary, we used a large volume of low-fidelity data to train a general and sufficiently large DNN model to extract the structural relationships between the stress and strain of idealized composites. We then fine-tuned the pre-trained model to increase the predictive accuracy using few but high-fidelity FEM data.

It is noteworthy that an ordinary neural network as in this study does not guarantee thermodynamic consistency, such as the monotonic increase of plastic work, or smooth stress-strain curves without non-physical fluctuation. To overcome such limitations, one can use a regularizer that constrains the space of admissible solutions [52,53], or restrict the function space over which the surrogate model is constructed [54,55]. However, falsely imposed assumption often entails a surrogate model with higher bias, and a specific neural network architecture constructed with a particular regularizer or behavior inductive bias cannot be easily transformed to task-specific models especially when the assumptions of the two tasks are different. For that reason, the proposed approach used the most flexible neural network architecture without any assumptions avoiding the misspecification of a model and allowing the pre-trained model to easily adapt to task-specific prediction models

4. Result and discussion

We used the DNN trained via transfer learning to predict the stress-strain curves of elasto-plastic composites. To evaluate the performance of transfer learning, the DNN model trained via transfer learning using both homogenization and FEM datasets was compared with the DNN model trained only with a small FEM dataset. The DNN architectures and initial weights of the two models were identical. In addition, we

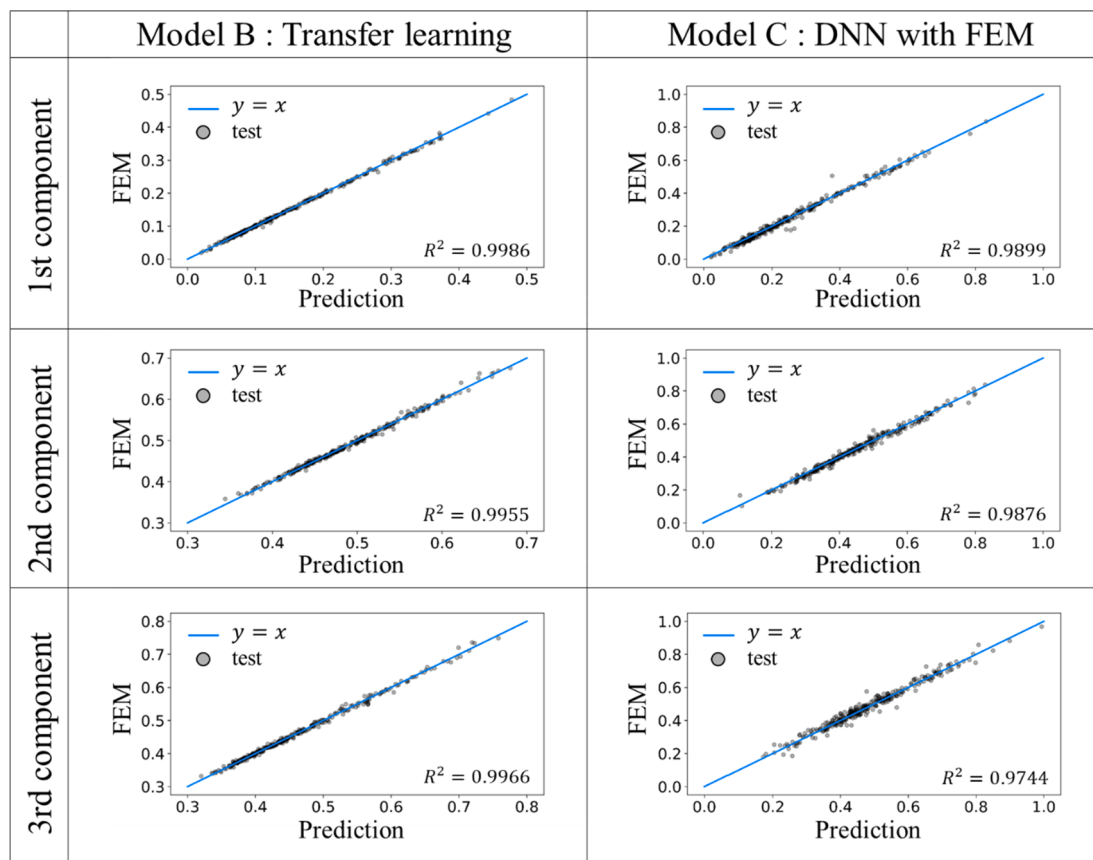


Fig. 6. Comparison between prediction (transfer learning/DNN with FEM) and ground truth (FEM) of the top three principal components. Model B refers to the model applying transfer learning. Model C refers to the model trained only with FEM data. 300 test data were used for comparison.

Table 2

Comparison of R^2 values for 10 principal components from Model B (transfer learning) and Model C (DNN with FEM).

	1st	2nd	3rd	4th	5th	6th	7th	8th	9th	10th
Model B	0.999	0.995	0.997	0.988	0.990	0.980	0.986	0.970	0.960	0.948
Model C	0.991	0.985	0.976	0.904	0.787	0.471	0.317	0.317	0.187	0.045

used the same training, validation, and test datasets from the FEM for both DNN models.

4.1. Ellipsoidal particle reinforced composite

We considered an ellipsoidal particle-reinforced composite subjected to uniaxial tensile loading. FEM data were generated using an RVE with reinforcement particles in the FCC configuration as shown in Fig. 2 (a, b). The prediction and ground truth of the top three principal components are compared between Models B and C in Fig. 6, which clearly shows that transfer learning is superior to direct training in predicting principal components. The comparison results for Model A are presented in Fig. S5 (see *Supplementary Information*). The R^2 values, which are statistical measurements representing how closely the regression fits the data, were much higher in Model B, as indicated in Table 2. In Model B, the R^2 values from transfer learning were remarkably high across all 10 principal components, while in Model C, the R^2 values decreased significantly for less important principal components. The maximum error of each stress-strain curve is defined as follows:

$$\text{Maximum Error} = \max\left(\frac{\sigma_1^{\text{Pred}} - \sigma_1^{\text{FEM}}}{\sigma_1^{\text{FEM}}}, \dots, \frac{\sigma_{101}^{\text{Pred}} - \sigma_{101}^{\text{FEM}}}{\sigma_{101}^{\text{FEM}}}\right). \quad (16)$$

The maximum error histogram is presented for 300 test data in Fig. 7.

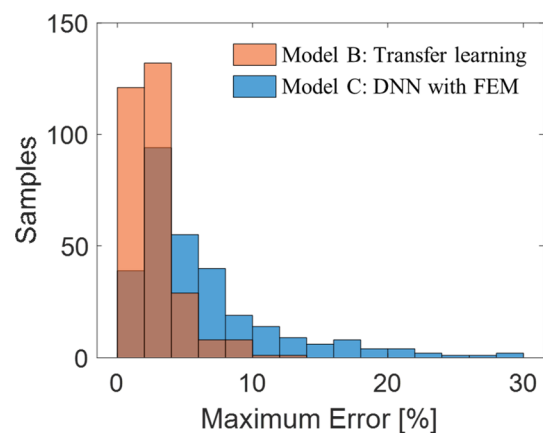


Fig. 7. Comparison between performances of transfer learning and DNN with FEM for ellipsoidal particle-reinforced composite. The error was defined as maximum relative error for each stress-strain curve prediction compared to ground truth (FEM). 300 test data were used for comparison.

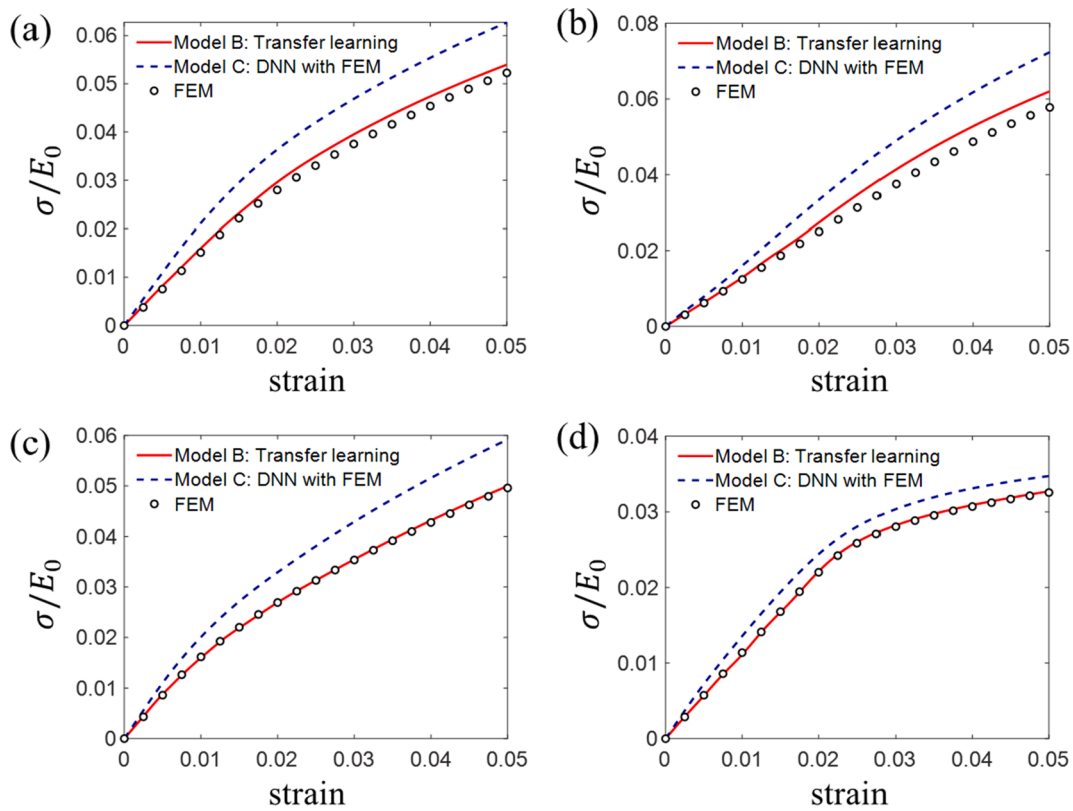


Fig. 8. Comparison between prediction (transfer learning/DNN with FEM) and ground truth (FEM) where DNN exhibited the top four maximum relative errors for ellipsoidal particle-reinforced composite.

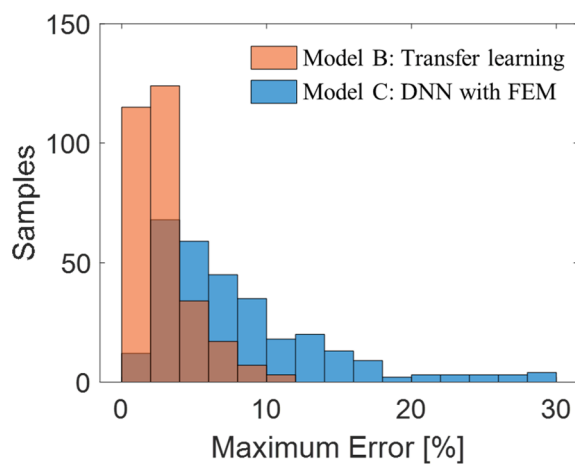


Fig. 9. Comparison between performances of transfer learning and DNN with FEM for short fiber-reinforced composite. The error was defined as maximum relative error for each stress-strain curve prediction compared to ground truth (FEM). 300 test data were used for comparison.

Model B, trained via transfer learning, outperformed Model C, which was directly trained with the FEM dataset. The predictions from both models are presented in Fig. 8 for the four cases in which model C exhibited the greatest errors. Transfer learning shows reliable predictions even for the worst cases. Moreover, Fig. S6 presents the four worst cases in which Model A, the DNN trained only with the homogenization dataset, exhibited the greatest errors (see [Supplementary Information](#)). The comparison between the results from Models A and B clearly shows that the DNN pre-trained with the homogenization dataset is fine-tuned appropriately via transfer learning.

4.2. Short fiber-reinforced composite

Homogenization theories based on Eshelby's solution assume that reinforcements are ellipsoidal. In this section, we verify whether transfer learning using homogenization data can be applied to a composite containing non-ellipsoidal reinforcements. The homogenization method has frequently been used to analyze composites having cylindrical or disk-shaped reinforcements with high aspect ratios [56,57]. In the present study, an FEA was performed on the FCC-structured RVE of a cylindrical short fiber-reinforced composite, as shown in Fig. 2 (c, d). We generated 2000 FEM data and divided them into training, validation, and test sets in a ratio of 1400:300:300. The same homogenization dataset as that mentioned in [Section 4.1](#) was used for transfer learning, that is, the DNN pre-trained by the homogenization dataset, where the ellipsoidal reinforcement was assumed, was fine-tuned with the FEM dataset on composites containing cylindrical short fiber-reinforcements. The maximum error histogram for the 300 test data is shown in Fig. 9. The predictions from both models are presented in Fig. 10 for the four cases in which Model C exhibited the greatest errors. Fig. S7 shows the predictions for the four cases in which Model A exhibited the greatest errors (see [supplementary information](#)). As described in [Section 4.1](#), Model B, trained via transfer learning, achieved the best predictive performance. These results confirm that transfer learning with homogenization data can also be applied to composites embedded with non-ellipsoidal reinforcements. For example, for composites containing flake-like reinforcements, such as graphene platelets, a DNN can be pre-trained using homogenization data generated by assuming oblate spheroid particle reinforcements; the DNN can then be fine-tuned with FEM data or experimental data via transfer learning.

4.3. Ellipsoidal particle reinforced composite under cyclic loading

Ellipsoidal particle-reinforced composites subjected to cyclic loading

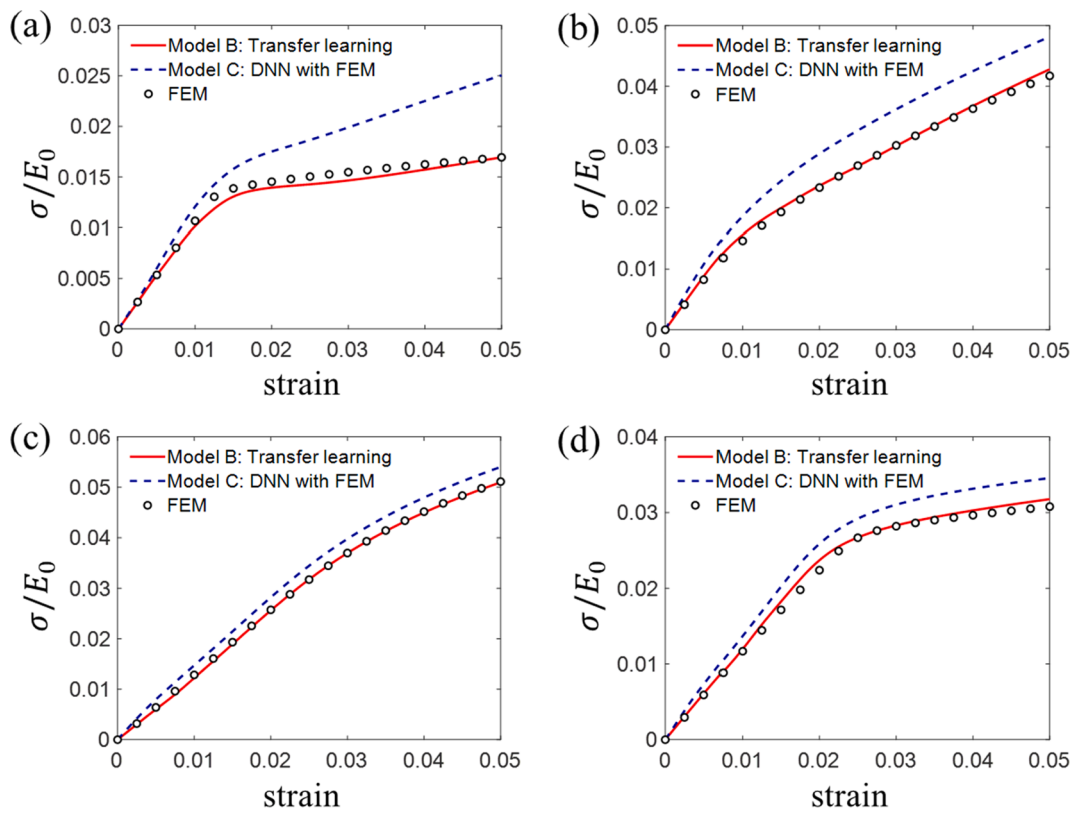


Fig. 10. Comparison between prediction (transfer learning/DNN with FEM) and ground truth (FEM) where DNN exhibited the top four maximum relative errors for short fiber-reinforced composite.

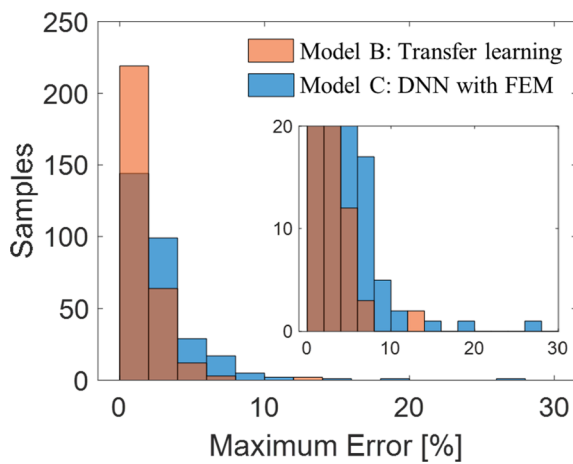


Fig. 11. Comparison between performances of transfer learning and DNN with FEM for ellipsoidal particle-reinforced composite under cyclic loading. The error was defined as the maximum relative error between prediction and ground truth (FEM) at maximum tension and compression. 300 test data were used for comparison.

were considered to further show the applicability of our transfer learning framework. The composites were stretched to 0.05 strain, compressed to -0.05 strain, and recovered to zero strain, which results in stress-strain curves with 401 strain steps from homogenization theory and FEM. For simplicity, we treated the stress-strain curves as 401-dimensional vectors, not as manifold data. Under cyclic loading conditions, 59,500 and 2000 stress-strain curve data were obtained from the homogenization method and FEM, respectively. The dataset from the homogenization methods was divided into training and validation sets in a ratio of 49,000:10,500, and the FEM data were divided into training,

validation, and test sets in a ratio of 1400:300:300. We used the DNN architecture considered in Section 3. The maximum relative error (Eq. (16)) used to compare the performances of the models in Section 4.1 and 4.2 is not appropriate for cyclic loading conditions because the denominator of Eq. (16) approaches near zero during the unloading process. In this section, the maximum relative error was calculated only at the maximum tension (0.05 strain) at strain step 101 and compression (-0.05 strain) at strain step 301 as shown in Eq. (17).

$$\text{Maximum Error} = \max \left(\frac{\sigma_{101}^{\text{Pred}} - \sigma_{101}^{\text{FEM}}}{\sigma_{101}^{\text{FEM}}}, \frac{\sigma_{301}^{\text{Pred}} - \sigma_{301}^{\text{FEM}}}{\sigma_{301}^{\text{FEM}}} \right). \quad (17)$$

The maximum error histogram for the 300 test data is shown in Fig. 11. The predictions from Model B and C are presented in Fig. 12 for the four cases in which Model C exhibited the greatest errors. Fig. S8 shows the predictions for the four cases in which Model A exhibited the greatest errors (see supplementary information). As in the previous sections, Model B, trained via transfer learning, showed better predictive performance over Model C. We note that the predictive performance under cyclic loading can be further improved after hyper-parameter optimization because the hyper-parameters of the DNN was optimized for uniaxial tension conditions via grid-search technique. Non-physical fluctuations were occasionally observed in the prediction of stress-strain curves, which is the limitation of neural networks and should be further improved in future works. In addition, considering a variety of loading modes and histories as input is another improvement to be made.

5. Conclusion

In this study, we demonstrated a transfer learning-based composite analysis technique that can efficiently exploit a large dataset based on the homogenization method when only a small dataset from FEM simulations or experiments is available because of high computational and

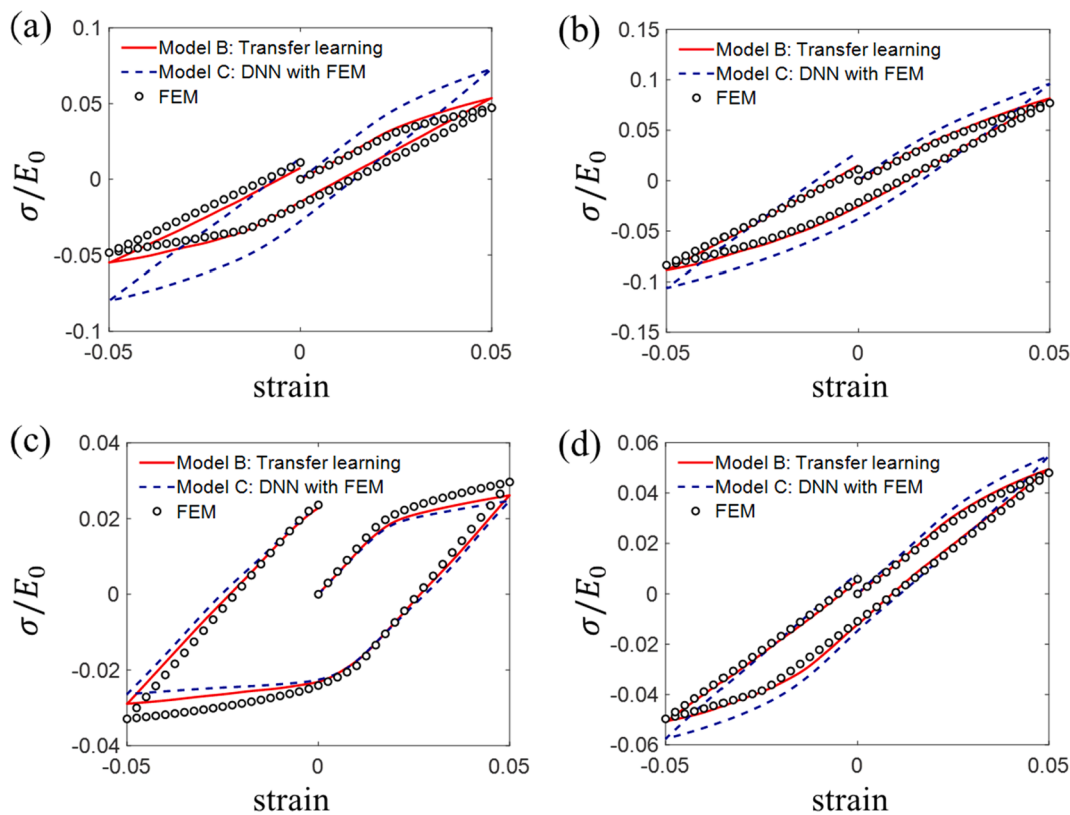


Fig. 12. Comparison between prediction (transfer learning/DNN with FEM) and ground truth (FEM) where DNN exhibited the top four maximum relative errors at maximum tension and compression for ellipsoidal particle-reinforced composite under cyclic loading.

economic costs. Because machine learning is a data-hungry technique, better generalization can be achieved with a greater amount of data. The homogenization theory has the advantage of providing a large amount of data at a lower cost and within a shorter time compared with the FEM or experimental methods, although its prediction accuracy is relatively inferior. Considering the task of predicting the elasto-plastic response of particle/short fiber-reinforced composites under uniaxial tension and cyclic loading, we demonstrated that the accuracy and efficiency of a composite analysis can be improved by training a DNN model with a large but less accurate dataset based on the homogenization method and then fine-tuning the DNN with an accurate but small dataset based on the FEM. Although we adopted the adaptive incrementally affine method to generate the homogenization data, several other homogenization theories can also be applied to the initial training dataset in the transfer learning scheme. The proposed method can easily be generalized to enable accurate and efficient prediction of various properties of composites with only a small, accurate dataset when any of the homogenization theories can determine the qualitative features of the composite.

CRediT authorship contribution statement

Jiyoung Jung: Conceptualization, Methodology, Investigation, Data curation, Software, Writing – original draft, Writing – review & editing. **Yongtae Kim:** Methodology, Investigation. **Jinkyoo Park:** Methodology, Software, Validation, Supervision, Writing – review & editing. **Seunghwa Ryu:** Conceptualization, Investigation, Validation, Supervision, Project administration, Writing – review & editing.

Declaration of Competing Interest

The authors declare that they have no known competing financial interests or personal relationships that could have appeared to influence

the work reported in this paper.

Acknowledgement

This research was supported by Basic Science Research Program (2019R1A2C4070690) and Creative Materials Discovery Program (2016M3D1A1900038) through the National Research Foundation of Korea (NRF) funded by the Ministry of Science and ICT (MIST) of the Republic of Korea, as well as the KAIST-funded Global Singularity Research Program for 2019 (N11190118).

Appendix A. Supplementary material

Supplementary data to this article can be found online at <https://doi.org/10.1016/j.compstruct.2022.115210>.

References

- [1] Eschelby JD. The determination of the elastic field of an ellipsoidal inclusion, and related problems. Proc R Soc Lond A 1957;241:376–96.
- [2] Mori T, Tanaka K. Average stress in matrix and average elastic energy of materials with misfitting inclusions. Acta Metall 1973;21(5):571–4.
- [3] Friebel C, Doghri I, Legat V. General mean-field homogenization schemes for viscoelastic composites containing multiple phases of coated inclusions. Int J Solids Struct 2006;43(9):2513–41.
- [4] Ryu S, Lee S, Jung J, Lee J, Kim Y. Micromechanics-based homogenization of the effective physical properties of composites with an anisotropic matrix and interfacial imperfections. Front Mater 2019;6:21.
- [5] Jung J, Lee S, Ryu B, Ryu S. Investigation of effective thermoelectric properties of composite with interfacial resistance using micromechanics-based homogenisation. Int J Heat Mass Transf 2019;144:118620. <https://doi.org/10.1016/j.ijheatmasstransfer.2019.118620>.
- [6] Pierard O, Friebel C, Doghri I. Mean-field homogenization of multi-phase thermo-elastic composites: a general framework and its validation. Compos Sci Technol 2004;64(10–11):1587–603.
- [7] Müller V, Kabel M, Andrä H, Böhlke T. Homogenization of linear elastic properties of short-fiber reinforced composites—A comparison of mean field and voxel-based methods. Int J Solids Struct 2015;67–68:56–70.

- [8] Naili C, Doghri I, Kanit T, Sukiman MS, Aissa-Berriaies A, Imad A. Short fiber reinforced composites: unbiased full-field evaluation of various homogenization methods in elasticity. *Compos Sci Technol* 2020;187:107942. <https://doi.org/10.1016/j.compscitech.2019.107942>.
- [9] Tian W, Qi L, Su C, Liang J, Zhou J. Numerical evaluation on mechanical properties of short-fiber-reinforced metal matrix composites: two-step mean-field homogenization procedure. *Compos Struct* 2016;139:96–103.
- [10] David Müzel S, Bonhin EP, Guimaraes NM, Guidi ES. Application of the Finite Element Method in the Analysis of Composite Materials: A Review. *Polymers* 2020; 12(4):818. <https://doi.org/10.3390/polym12040818>.
- [11] Dey A. Machine learning algorithms: a review. *Int. J. Comput. Sci. Inform. Technol.* 2016;7:1174–9.
- [12] Wang H, Ma C, Zhou L. A brief review of machine learning and its application. In: 2009 International conference on information engineering and computer science: IEEE; 2009. p. 1–4.
- [13] Liu X, Tian S, Tao F, Du H, Yu W. Machine learning-assisted modeling of composite materials and structures: a review. *AIAA Scitech 2021 Forum* 2021:2023.
- [14] Chen C-T, Gu GX. Machine learning for composite materials. *MRS Commun* 2019;9 (2):556–66.
- [15] Yang C, Kim Y, Ryu S, Gu GX. Prediction of composite microstructure stress-strain curves using convolutional neural networks. *Mater Des* 2020;189:108509. <https://doi.org/10.1016/j.matdes.2020.108509>.
- [16] Yang C, Kim Y, Ryu S, Gu GX. Using convolutional neural networks to predict composite properties beyond the elastic limit. *MRS Commun* 2019;9(2):609–17.
- [17] Chen T, Dvorak GJ, Benveniste Y. Mori-Tanaka Estimates of the Overall Elastic Moduli of Certain Composite Materials. *J Appl Mech* 1992;59:539–46.
- [18] McLaughlin R. A study of the differential scheme for composite materials. *Int J Eng Sci* 1977;15(4):237–44.
- [19] Norris AN. A differential scheme for the effective moduli of composites. *Mech Mater* 1985;4(1):1–16.
- [20] Hori M, Nemat-Nasser S. Double-inclusion model and overall moduli of multi-phase composites. *Mech Mater* 1993;14(3):189–206.
- [21] Doghri I, Adam L, Bilger N. Mean-field homogenization of elasto-viscoplastic composites based on a general incrementally affine linearization method. *Int J Plast* 2010;26(2):219–38.
- [22] Miled B, Doghri I, Brassart L, Delannay L. Micromechanical modeling of coupled viscoelastic-viscoplastic composites based on an incrementally affine formulation. *Int J Solids Struct* 2013;50(10):1755–69.
- [23] Wu L, Noels L, Adam L, Doghri I. A combined incremental-secant mean-field homogenization scheme with per-phase residual strains for elasto-plastic composites. *Int J Plast* 2013;51:80–102.
- [24] Wu L, Noels L, Adam L, Doghri I. An implicit-gradient-enhanced incremental-secant mean-field homogenization scheme for elasto-plastic composites with damage. *Int J Solids Struct* 2013;50(24):3843–60.
- [25] Jung J, Kim Y, Lee S, Doghri I, Ryu S. Improved incrementally affine method for viscoelastic-viscoplastic composite by utilizing an adaptive scheme. *engrXiv*: 1031224/osf.io/fu3ja. 2021.
- [26] Kim Y, Jung J, Lee S, Doghri I, Ryu S. Adaptive Affine Homogenization Method for Visco-hyperelastic Composites with Interfacial Damage. *engrXiv*:1031224/osf.io/3jybz. 2021.
- [27] Gu GX, Chen C-T, Buehler MJ. De novo composite design based on machine learning algorithm. *Extreme Mech Lett* 2018;18:19–28.
- [28] Gu GX, Chen C-T, Richmond DJ, Buehler MJ. Bioinspired hierarchical composite design using machine learning: simulation, additive manufacturing, and experiment. *Mater Horiz* 2018;5(5):939–45.
- [29] Abueidda DW, Almasri M, Ammourah R, Ravaioli U, Jasliuk IM, Sobh NA. Prediction and optimization of mechanical properties of composites using convolutional neural networks. *Compos Struct* 2019;227:111264. <https://doi.org/10.1016/j.comstruct.2019.111264>.
- [30] Mentges N, Dashtbozorg B, Mirkhalaf SM. A micromechanics-based artificial neural networks model for elastic properties of short fiber composites. *Compos B Eng* 2021;213:108736. <https://doi.org/10.1016/j.compositesb.2021.108736>.
- [31] Rao C, Liu Y. Three-dimensional convolutional neural network (3D-CNN) for heterogeneous material homogenization. *Comput Mater Sci* 2020;184:109850. <https://doi.org/10.1016/j.commatsci.2020.109850>.
- [32] Torrey L, Shavlik J. Transfer learning. Handbook of research on machine learning applications and trends: algorithms, methods, and techniques. In: Olivas ES, Guerrero JDM, Martinez-Sober M, Magdalena-Benedito JR, Serrano López AJ, editors. Handbook of research on machine learning applications and trends: algorithms, methods, and techniques. IGI Global; 2010. p. 242–64. <https://doi.org/10.4018/978-1-60566-766-9.ch011>.
- [33] Shin H-C, Roth HR, Gao M, Lu Le, Xu Z, Nogues I, et al. Deep convolutional neural networks for computer-aided detection: CNN architectures, dataset characteristics and transfer learning. *IEEE Trans Med Imaging* 2016;35(5):1285–98.
- [34] Zheng X, Zheng P, Zhang R-Z. Machine learning material properties from the periodic table using convolutional neural networks. *Chem Sci* 2018;9(44): 8426–32.
- [35] Hussain M, Bird JJ, Faria DR. A study on cnn transfer learning for image classification. UK Workshop on computational Intelligence: Springer; 2018. p. 191–202.
- [36] Han D, Liu Q, Fan W. A new image classification method using CNN transfer learning and web data augmentation. *Expert Syst Appl* 2018;95:43–56.
- [37] Prajapati SA, Nagaraj R, Mitra S. Classification of dental diseases using CNN and transfer learning. In: 2017 5th International Symposium on Computational and Business Intelligence (ISCBIB): IEEE; 2017. p. 70–4.
- [38] Masson R. New explicit expressions of the Hill polarization tensor for general anisotropic elastic solids. *Int J Solids Struct* 2008;45(3-4):757–69.
- [39] Doghri I, Brassart L, Adam L, Gérard J-S. A second-moment incremental formulation for the mean-field homogenization of elasto-plastic composites. *Int J Plast* 2011;27(3):352–71.
- [40] DIGIMAT. e-Xstream engineering. www-xstreamcom; 2016.
- [41] Abaqus F. Abaqus inc. Providence, Rhode Island, United States; 2017.
- [42] Tian W, Qi L, Chao X, Liang J, Fu M. Periodic boundary condition and its numerical implementation algorithm for the evaluation of effective mechanical properties of the composites with complicated micro-structures. *Compos B Eng* 2019;162:1–10.
- [43] Chao X, Qi L, Cheng J, Tian W, Zhang S, Li H. Numerical evaluation of the effect of pores on effective elastic properties of carbon/carbon composites. *Compos Struct* 2018;196:108–16.
- [44] Ge J, Qi L, Chao X, Xue Y, Hou X, Li H. The effects of interphase parameters on transverse elastic properties of Carbon-Carbon composites based on FE model. *Compos Struct* 2021;268:113961. <https://doi.org/10.1016/j.comstruct.2021.113961>.
- [45] Chollet F. Keras: The python deep learning library. *Astrophysics Source Code Library*. 2018:ascl:1806.022.
- [46] Ioffe S, Szegedy C. Batch normalization: Accelerating deep network training by reducing internal covariate shift. International Conference On Machine Learning: PMLR; 2015. p. 448–56.
- [47] Santurkar S, Tsipras D, Ilyas A, Madry A. How does batch normalization help optimization? *arXiv preprint arXiv:180511604*; 2018.
- [48] Pedamonti D. Comparison of non-linear activation functions for deep neural networks on MNIST classification task. *arXiv preprint arXiv:180402763*; 2018.
- [49] Nwankpa C, Ijomah W, Gachagan A, Marshall S. Activation functions: Comparison of trends in practice and research for deep learning. *arXiv preprint arXiv: 181103378*; 2018.
- [50] Hendrycks D, Gimpel K. Gaussian error linear units (gelus). *arXiv preprint arXiv: 160608415*; 2016.
- [51] Kingma DP, Ba J. Adam: A method for stochastic optimization. *arXiv preprint arXiv:14126980*; 2014.
- [52] Raissi M, Perdikaris P, Karniadakis GE. Physics-informed neural networks: A deep learning framework for solving forward and inverse problems involving nonlinear partial differential equations. *J Comput Phys* 2019;378:686–707.
- [53] Karniadakis GE, Kevrekidis IG, Lu Lu, Perdikaris P, Wang S, Yang L. Physics-informed machine learning. *Nat Rev Phys* 2021;3(6):422–40.
- [54] Amos B, Xu L, Kolter JZ. Input convex neural networks. International Conference on Machine Learning: PMLR 2017:146–55.
- [55] Wehenkel A, Louppe G. Unconstrained monotonic neural networks. *Adv Neural Inform Process Syst* 2019;32:1545–55.
- [56] Wan C, Chen B. Reinforcement and interphase of polymer/graphene oxide nanocomposites. *J Mater Chem* 2012;22(8):3637. <https://doi.org/10.1039/c2jm15062j>.
- [57] Yoo Y, Spencer MW, Paul DR. Morphology and mechanical properties of glass fiber reinforced Nylon 6 nanocomposites. *Polymer* 2011;52(1):180–90.